Proceedings of the ASME 2021
Fluids Engineering Division Summer Meeting
FEDSM2021
August 10-12, 2021, Virtual, Online

FEDSM2021-65655

WAKE STRUCTURES AND EFFECT OF HYDROFOIL SHAPES IN EFFICIENT FLAPPING PROPULSION

John Kelly
Department of Mechanical and Aerospace Engineering,
University of Virginia
Charlottesville, VA

Pan Han
Department of Mechanical and Aerospace Engineering,
University of Virginia
Charlottesville, VA

Haibo Dong
Department of Mechanical and Aerospace Engineering,
University of Virginia
Charlottesville, VA

Tyler Van Buren
Department of Mechanical Engineering,
University of Delaware
Newark, DE

ABSTRACT

In this work, direct numerical simulation (DNS) is used to investigate how airfoil shape affects wake structure and performance during a pitching-heaving motion. First, a class-shape transformation (CST) method is used to generate airfoil shapes. CST coefficients are then varied in a parametric study to create geometries that are simulated in a pitching and heaving motion via an immersed boundary method-based numerical solver. The results show that most coefficients have little effect on the propulsive efficiency, but the second coefficient does have a very large effect. Looking at the CST basis functions shows that the effect of this coefficient is concentrated near the 25% mark of the foils chord length. By observing the thrust force and hydrodynamic power through a period of motion it is shown that the effect of the foil shape change is realized near the middle of each flapping motion. Through further inspection of the wake structures, we conclude that this is due to the leading-edge vortex attaching better to the foil shapes with a larger thickness around 25% of the chord length. This is verified by the pressure contours, which show a lower pressure along the leading edge of the better performing foils. The more favorable pressure gradient generated allows for higher efficiency motion.

Keywords: direct numerical simulation, immersed boundary method, flapping propulsion, hydrofoil shape, wakes

NOMENCLATURE

a_i	coefficients of CST
h	heaving position
h_0	heaving amplitude
f	motion frequency
t	time
T	period of motion
θ	pitching angle
θ_0	pitching amplitude
ϕ	phase angle between pitching and heaving
c	foil chord length
ν	kinematic viscosity
U_∞	freestream velocity
Re	Reynolds number, $Re = U_\infty c/\nu$
f^*	reduced frequency, $f^* = fc/U_\infty$
A	tail tip peak-to-peak amplitude
St	Strouhal number, $St = fA/U_\infty$
F	thrust force
P	hydrodynamic power
ρ	fluid density
C_T	thrust coefficient, $C_T = F/(0.5\rho U_\infty^2 c^2)$
C_P	power coefficient, $C_P = P/(0.5\rho U_\infty^3 c^2)$
η	propulsive efficiency, $\eta = C_T/C_P$
ω_Z	z – vorticity
p	pressure
C_{pr}	pressure coefficient, $C_{pr} = p/(0.5\rho U_\infty^2)$

1. INTRODUCTION

Airfoils are surfaces used in wings, fins, and stabilizers of flying and swimming objects that are designed to create favorable lift-to-drag ratios during flight. Flying vehicle performance has been greatly enhanced by optimizing the shape of the airfoil's cross section to improve lift and propulsive efficiency. Recent research has shown a shift in focus toward unsteady hydrodynamic propulsion and leverages methods used by fish and other animals to achieve high efficiency propulsion [1-3]. Bio-inspired flapping propulsion has the capability of achieving better efficiencies through range of flow regimes and motion applications [4]. Additionally, previous studies have exemplified flapping foil's shape can have a significant impact on foil performance [5]. The goal of this research is to further characterize the role of variable foil shape on performance during a flapping motion.

In this study, we use a CST parameterization method to create geometric parameters that are varied to create unique foil shapes. We then prescribe a flapping motion and flow conditions in the range of the ones seen in dolphin swimming. Computational fluid dynamics (CFD) simulations of these shapes in a flapping motion were completed using an in-house immersed boundary method-based DNS solver. The results are used to study their performance and wake structures. From this study it is shown that the most important part of the foil thickness for propulsive efficiency is around 25% of the chord length. Optimizing this region alone shows about a 12% gain in efficiency from the NACA0012 foil shape. A deeper dive into the continuous coefficients of thrust and power through a period of motion shows that the gains in efficiency seen by increasing the foil thickness near the 25% mark occurs primarily in the middle portion of the flapping motion. This efficiency comes from a lower pressure on the leading edge of the foil in the middle of each stroke. The lower pressure occurs because the leading-edge vortex is better attached, whereas in the lower efficiency cases it separates from the foil body.

2. METHODS

2.1 Class-Shape Transformation Parameterization

The parametric study begins by using the CST parameterization method to create airfoil geometries. In this method, a class function defines the basic foil shape, and a shape function allows modification of that shape to create each foil. The method was developed by Kulfan [6,7], and was chosen because previous studies identified it as an efficient method for foil shapes while maintaining core foil shapes [5,8]. Based on previous work of Han et al. [5], here, we similarly keep the class function the same and use six coefficients for the shape function (a_0, a_1, … a_5). The airfoil shape is derived as:

$$B_j = K_j^N \cdot x^{j+0.5} \cdot (1-x)^{N-j+1} \quad (1)$$

$$K_j^N = \frac{N!}{j!(N-j)!} \quad (2)$$

$$y(x) = \sum_{j=0}^{N} a_j \cdot B_j \quad (3)$$

where B is the basis function, N is one less than the number of basis functions, and $y(x)$ defines the foil shape. The basis function resulting from each individual term is shown in Fig. 1, and the foil is created by summing the product of each coefficient with the corresponding basis function.

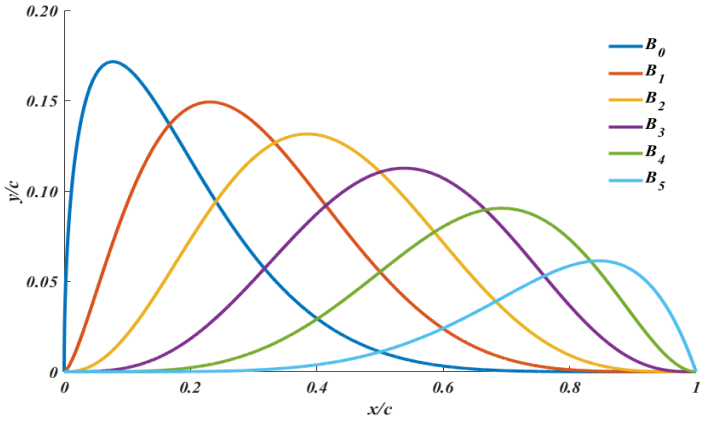

FIGURE 1: Shape of basis functions of CST with 6 parameters

In the previous work of Han et al. [5], using NACA0012 as a starting point, an optimization process is employed to optimize the propulsive efficiency of a pitching-heaving airfoil at reduced frequency 0.4 and Reynolds number 10000. The CST coefficients of NACA0012 airfoil and the obtained optimized airfoil are listed in Table 1.

	a_0	a_1	a_2	a_3	a_4	a_5
NACA0012	0.17037	0.16020	0.14364	0.16642	0.11047	0.17943
Optimized	0.22669	0.34367	0.30546	0.33860	0.15468	0.19981

TABLE 1: CST parameters for NACA0012 and optimized foil shapes

For this study, the CST coefficients of the studied airfoils are generated from that of the NACA0012 and optimized airfoils, with the equation below:

$$a_n = a_{n-B} + 0.25(a_{n-O} - a_{n-B})(i), \quad (4)$$

where a_n is the *nth* parameter of the required airfoil, a_{n-B} is the *nth* parameter of the NACA0012 foil and a_{n-O} is the *nth* parameter of the optimized foil. With i changing from 0 to 6, different a_n can be obtained to generate airfoil with different thickness. For example, when $i = 4$ for $a_n(n = 0, 1, \ldots, 5)$, the generated foil will be the optimized airfoil.

However, in the current work, to focus on the effects of each coefficient, all other parameters are held at the NACA0012 value while only one parameter is changed with the above formula. This results in each parameter varying from the NACA0012 value (i = 0) through the optimized shape value (i = 4) to the maximum value of equation (4) (i = 6). This is demonstrated in Fig. 2, which shows the foil shapes generated by varying the a_1

parameter while holding the other parameters at the NACA0012 value.

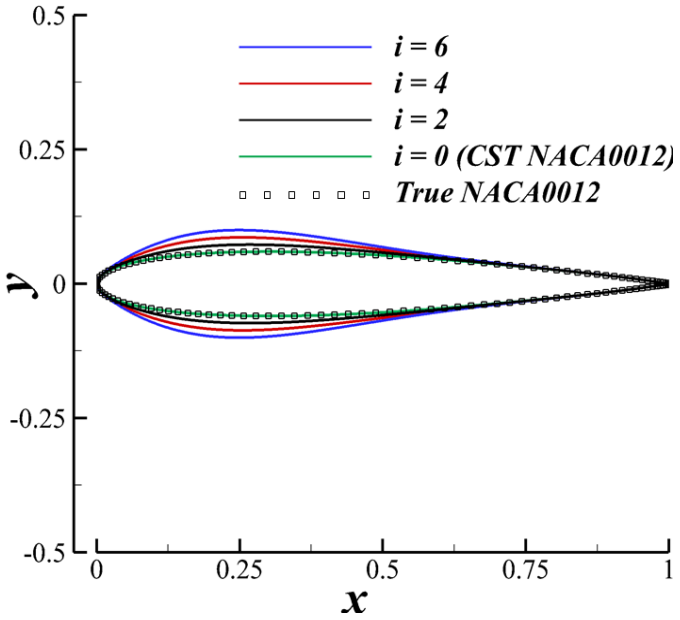

FIGURE 2: CST generated airfoils varying the a_1 parameter

Through the CST method, the airfoil is broken down into six coefficients that correspond to thickness at different points along the chord of the airfoil. The CST maintains the core airfoil shape and allows changes in the thickness in specific regions of the airfoil with just six inputs. Our parametric study design yields 36 unique foil shapes to compare the effect of varying each parameter on the foil performance.

2.2 Case Setup

After obtaining the foil shape from the CST as detailed above a sinusoidal pitching and heaving motion to the foils is prescribed. This motion is detailed in equations (5) and (6), with a pitching amplitude (θ_0) of 15º, a heaving amplitude (h_0) of 0.375, and a phase difference between the pitching and heaving angles (ϕ) of 270º. These values were chosen to be within the range of natural swimmers, such as fish.

$$h = h_0 \sin(2\pi ft) \quad (5)$$

$$\theta = \theta_0 \sin(2\pi ft + \phi) \quad (6)$$

Further details on the pitching and heaving motion are available in Buren [9].

The thrust force (F) and hydrodynamic power (P), which are used to calculate the propulsive efficiency (η), are computed using an in-house DNS CFD solver. This solver discretizes the two-dimensional incompressible Navier-Stokes equations using a cell-centered collocated arrangement of the primitive variables and solves the equations using a finite difference-based immersed boundary method on Cartesian grids [10]. An immersed boundary method is selected to allow a fixed mesh through the flapping motion rather than It has previously been applied to flapping propulsion simulations successfully [11, 12] and validated in previous works [13].

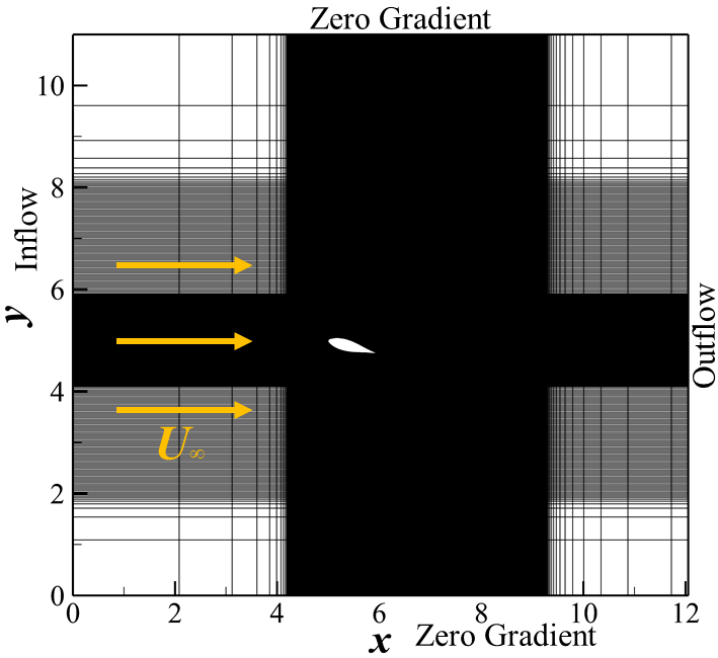

FIGURE 3: Case setup, detailed in Han et. al. [5]

The flow simulation is then set up with the computational grid and boundary conditions shown in Fig. 3. The left side of the domain has a prescribed inlet velocity. The top and bottom of the domain are defined by a zero-gradient boundary. The outflow on the right side of the domain also has a zero-gradient boundary. For this study, the flow conditions are described by two dimensionless parameters, the Reynolds number (Re) and the reduced frequency (f^*). The Reynolds number is chosen to be 10000, and the reduced frequency is 0.4, which are the same with previous work of Han et al. [5]. These values were also chosen to be within the natural domain [14, 15]. Also, in consideration of natural features, only symmetric airfoils are studied.

3. RESULTS

3.1 Efficiency

To understand our results, we first calculated the coefficient of thrust:

$$C_T = F/(0.5\rho U_\infty^2 c^2) \quad (7)$$

where ρ is fluid density, U_∞ is free stream velocity and c is the foil chord length. We then averaged C_T over one period of motion for each foil. The results are normalized by the average value in the NACA0012 case and are shown in Fig. 4a. The process was then repeated for the coefficient of power:

$$C_P = P/(0.5\rho U_\infty^3 c^2) \quad (8)$$

and the normalized averaged results are shown in Fig. 4b. Finally, we used these values to compute the propulsive efficiency for each case:

$$\eta = C_T/C_P \quad (9)$$

and normalized the results by the NACA0012 value. The outcome is plotted in Fig. 4c.

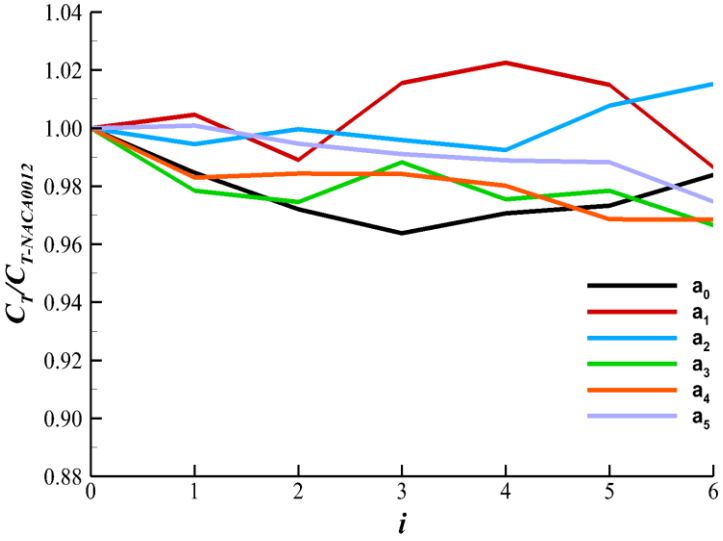

FIGURE 4a: Normalized coefficient of thrust (C_T) for each case

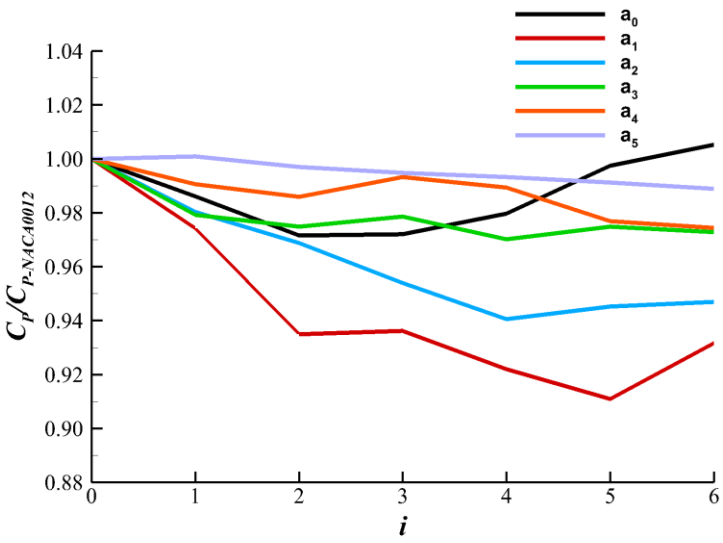

FIGURE 4b: Normalized coefficient of power (C_P) for each case

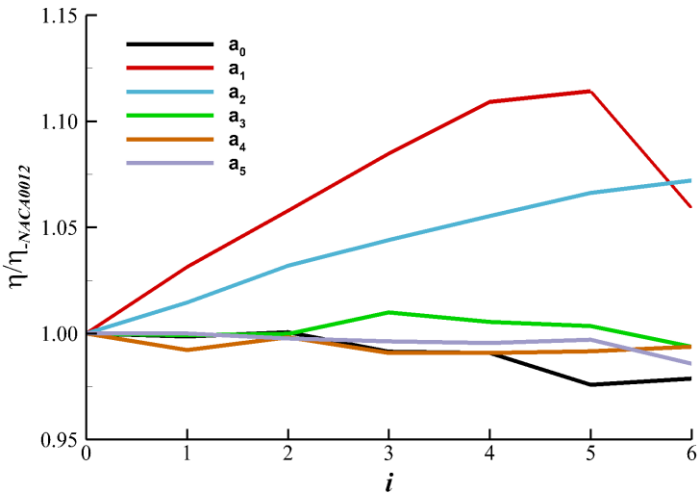

FIGURE 4c: Normalized efficiency (η) for each case

From Fig. 4c, parameter a_1 has the largest effect on propulsive efficiency. Parameter a_2 also has a significant effect. The remainder of the parameters seem to have very little effect on the total efficiency. The highest efficiencies occur when a_1 is at the i = 4 to i = 5 range. Looking at Fig. 4a, it is shown that in the i = 3 to i = 5 range of a_1 there is a slight increase in the thrust coefficient. All the other parameters show some decrease in thrust as the coefficient values increase. In Fig. 4b we see that a_1 had the lowest coefficient of power, especially in the i = 4 to i = 6 range. Parameter a_2 also shows values lower than the other coefficients. The percentage change in the power coefficient is larger than the change in the thrust coefficient in general, so the parameters with a lower C_P also show the highest efficiency. From this data, we are most interested in the a_1, i = 4 case, which had significant performance increases in efficiency and has the peak thrust value.

In Fig. 1, we see that a_1 and a_2 are concentrated near the front of the airfoil chord length, primarily from 15% to 35% of the chord length. This means for foil performance; the thickness of the airfoil is most important in that range.

3.2 NACA0012 vs a_1, i = 4

To further understand these cases and why there is a performance increase, we first look at the coefficient of thrust and coefficient of power over a one period of motion for both the a_1, i = 4 and the NACA0012 foils as plotted in Fig. 5a and Fig. 5b. In Fig. 5a, the thrust coefficients are very similar, with the main deviation starting at t/T = 0.55. Therefore, the improvements in thrust occur just before the middle of the flapping motion, as the foil begins to start the next stroke. In Fig. 5b, the power coefficients deviate more than the thrust coefficients. The values deviate most in the t/T = 0.45 to 0.65 range. There is a significant separation point at t/T = 0.45. The improvements in the power coefficient also occurs around the middle of the flapping motion, corresponding to just after the foil crosses the y = 5 line in the domain shown in Fig. 3.

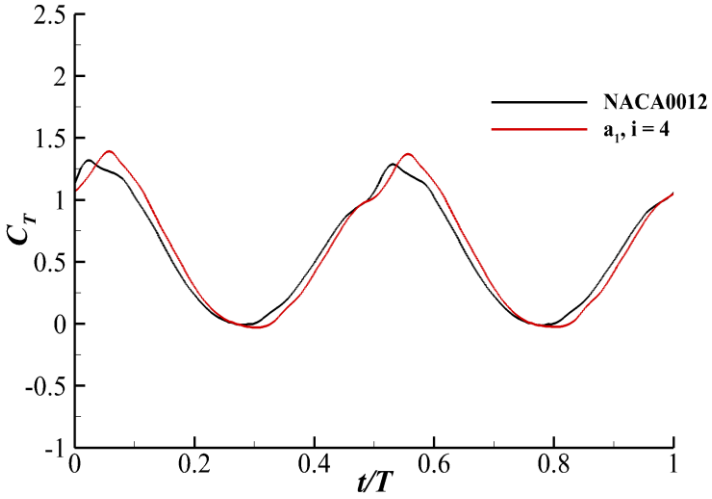

FIGURE 5a: Continuous coefficients of thrust over one period of motion for NACA0012 and a_1, i = 4

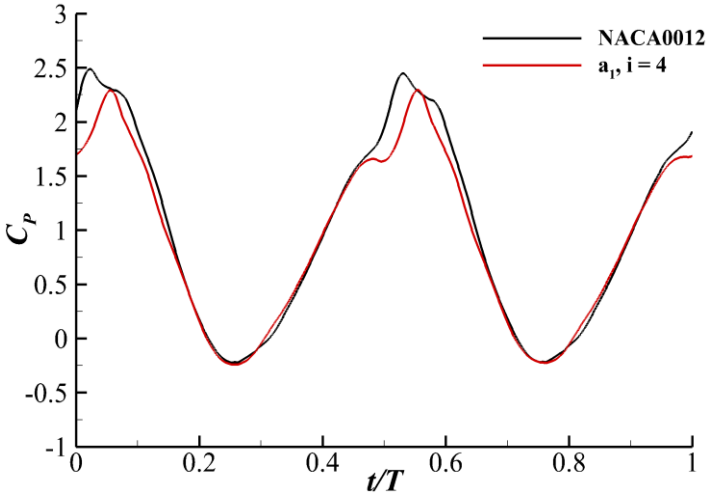

FIGURE 5b: Continuous coefficients of power over one period of motion for NACA0012 and a_1, i = 4

To understand the reason for the deviation of the power coefficient around t/T = 0.5, the wake structures of the NACA0012 and a_1, i = 4 foils are studied. The contour plots in Fig. 6 show the vorticity (ω_Z) of each foil at t/T = 0.5. A significant difference can be seen between the two contours on the leading (bottom) edge. In the NACA0012 case, the large vortex is entirely separated from the main body of the foil. In the a_1, i = 4 case, the large vortex is still fully attached to the foil body. The earlier separation of the leading-edge vortex causes the lower efficiency seen in the NACA0012 case. The pressure contours near the foil surface are studied to understand why the difference in the leading-edge vortex separation has a large effect on the foil efficiency. First, we compute the pressure coefficient values:

$$C_{pr} = p/(0.5\rho U_\infty^2) \qquad (10)$$

Contours of the normalized pressures are then plotted in Fig. 7. From these plots we see that the a_1, i = 4 foil has lower pressures than the NACA0012 foil along the back half of its leading edge. As the motion continues, moving into a lower pressure gives a lower hydrodynamic power. This gives the results that we see in Fig. 5b and Fig. 4b.

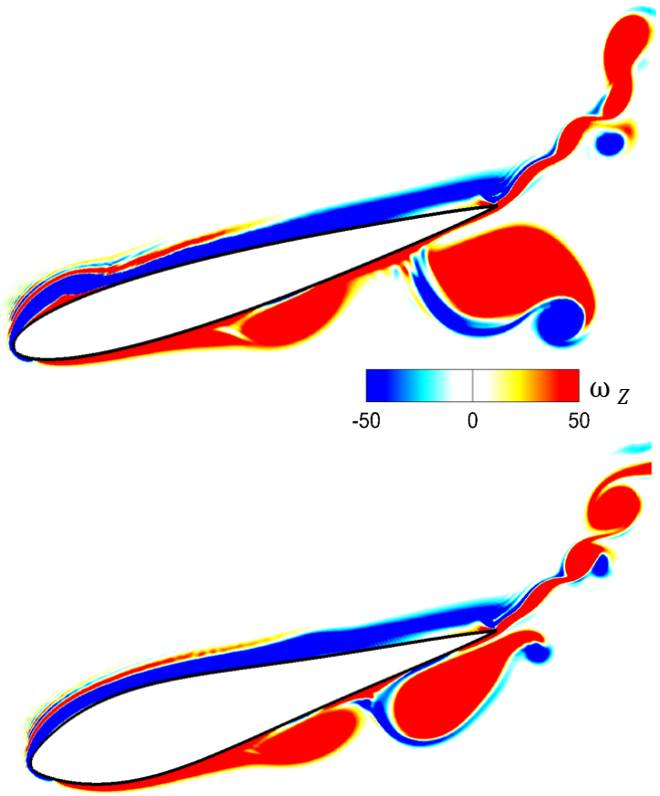

FIGURE 6: Vorticity contours (ω_Z) of the wake of the NACA0012 (TOP) and a_1, i = 4 (BOTTOM) foils at t/T = 0.5

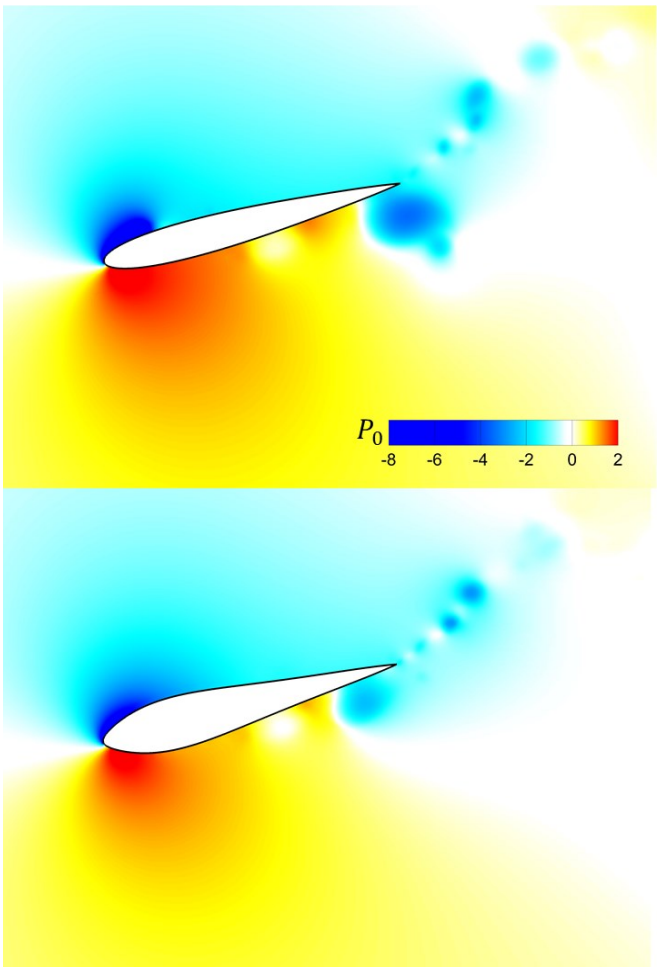

FIGURE 6: Pressure coefficient (C_{pr}) contours on the NACA0012 (TOP) and a_1, i = 4 (BOTTOM) foils at t/T = 0.5

4. CONCLUSION

In this study, a computational study flapping airfoils has been done using an in-house immersed boundary method-based numerical solver to investigate the effects of foil shape on efficiency and wake structure. Using the CST parameterization method to define airfoil shapes, it was shown that the most important part of the foil thickness for propulsive efficiency is about 25% of the chord length. We also discovered that the difference occurs mainly in the middle part of the stroke, just after passing the half-stroke point. Finally, we concluded that the changes in performance occur because of delayed vortex separation on the leading edge of the airfoil, creating a favorable pressure gradient allowing for higher efficiency motion. These results can be used to better understand the flapping airfoil seen in nature and will assist in future developments of vehicles that utilize flapping foils for propulsion. This study shows the effect of foil shapes in only one flow regime and with fixed flapping kinematics. Future studies are needed to understand how changing the shape along with the Reynolds number, Strouhal number, and flapping kinematics affects the foil performance.

ACKNOWLEDGEMENTS

This work was supported by ONR MURI N0014-14-1-0533, NSF CNS -1931929, and the NSF NRT program.

REFERENCES

[1] T. Van Buren, D. Floryan, A. J. Smits, P. Han, A. T. Bode-Oke, and H. Dong, “Optimizing foil shape for efficient unsteady propulsion,” *AIAA Scitech 2019 Forum*, no. January, pp. 1–9, 2019, doi: 10.2514/6.2019-1379.

[2] J. Wang, D. K. Wainwright, R. E. Lindengren, G. V. Lauder, and H. Dong, “Tuna locomotion: A computational hydrodynamic analysis of finlet function,” *J. R. Soc. Interface*, vol. 17, no. 165, 2020, doi: 10.1098/rsif.2019.0590.

[3] P. Han, G. V. Lauder, and H. Dong, “Hydrodynamics of median-fin interactions in fish-like locomotion: Effects of fin shape and movement,” *Phys. Fluids*, vol. 32, no. 1, 2020, doi: 10.1063/1.5129274.

[4] M. S. Triantafyllou, G. S. Triantafyllou, and D. K. P. Yue, “HYDRODYNAMICS OF FISHLIKE SWIMMING M.,” *Annu. Rev. Fluid Mech.*, vol. 32, pp. 33–53, 2000.

[5] P. Han, A. T. Bode-Oke, H. Dong, T. Van Buren, D. Floryan, and A. J. Smits, “Comparison of Geometric Parameterization Methods for Optimal Shape Design in Efficient Flapping Propulsion,” *AIAA Aviat. Forum*, no. June, pp. 1–8, 2019, doi: 10.2514/6.2019-3339.

[6] B. M. Kulfan, “Universal parametric geometry representation method,” *J. Aircr.*, vol. 45, no. 1, pp. 142–158, 2008, doi: 10.2514/1.29958.

[7] B. M. Kulfan and J. E. Bussoletti, “‘Fundamental’ parametric geometry representations for aircraft component shapes,” *Collect. Tech. Pap. - 11th AIAA/ISSMO Multidiscip. Anal. Optim. Conf.*, vol. 1, pp. 547–591, 2006, doi: 10.2514/6.2006-6948.

[8] D. A. Masters, N. J. Taylor, T. C. S. Rendall, C. B. Allen, and D. J. Poole, “Geometric comparison of aerofoil shape parameterization methods,” *AIAA J.*, vol. 55, no. 5, pp. 1575–1589, 2017, doi: 10.2514/1.J054943.

[9] T. Van Buren, D. Floryan, and A. J. Smits, “Scaling and performance of simultaneously heaving and pitching foils,” *AIAA J.*, vol. 57, no. 9, pp. 3666–3677, 2019, doi: 10.2514/1.J056635.

[10] D. A. Masters, N. J. Taylor, T. C. S. Rendall, C. B. Allen, and D. J. Poole, “Geometric comparison of aerofoil shape parameterization methods,” *AIAA J.*, vol. 55, no. 5, pp. 1575–1589, 2017, doi: 10.2514/1.J054943.

[11] P. Han, G. Liu, Y. Ren, and H. Dong, “Computational Analysis of 3D Fin-Fin Interaction in Fish’s Steady Swimming,” *FEDSM2016-7699*, pp. 1–6, 2016.

[12] P. Han, J. Wang, and H. Dong, “Effects of intermittent swimming gait in fish-like locomotion,” *AIAA Scitech 2020 Forum*, vol. 1 PartF, no. January, pp. 1–9, 2020, doi: 10.2514/6.2020-1779.

[13] Graham K. Taylor, Robert L. Nudds, and Adrian L. R. Thomas, “Flying and swimming animals cruise at a Strouhal

number tuned for high power efficiency," *Nature*, vol. 425, no. 6959, pp. 705–707, 2003, doi: 10.1038/nature02047.1.

[14] H. Dong, A. T. Bode-Oke, and C. Li, "Learning from Nature: Unsteady Flow Physics in Bioinspired Flapping Flight," *Flight Physics-Models, Tech. Technol. IntechOpen.*, pp. 1–18, 2018, [Online].

[15] C. Li, H. Dong, and G. Liu, "Effects of a dynamic trailing-edge flap on the aerodynamic performance and flow structures in hovering flight," *J. Fluids Struct.*, vol. 58, pp. 49–65, 2015, doi: 10.1016/j.jfluidstructs.2015.08.001.